Mathematical and experimental evaluation of a mini-channel PV/T and thermal panel in summer mode

Jinzhi Zhou[b, a], Xudong Zhao[c, a, *], Yanping Yuan[b], Yi Fan[a], Jing Li[a]

[a]School of Engineering and Computer Science, University of Hull, Hull, UK

[b]School of Mechanical Engineering, Southwest Jiaotong University, Chengdu, China

[c]Department of Power Engineering, North China Electric and Power Engineering, Baoding, China

Corresponding email: Xudong.Zhao@hull.ac.uk

Abstract: In this paper, a mini-channel PV/T and mini-channel thermal panel hot water system is presented. The thermal panels in this system use mini-channel tube as the heat exchanger, which has a small hydraulic diameter and large heat exchanger area, and this special structure can improve the heat transfer coefficient at the same flow rate than the conventional type. The performance of this system for generating hot water and electricity in summer has been tested, and a simulation model of this operating mode has been developed. Based on a typical day's weather data, the simulation model is verified, and the experimental and simulated results agree with each other very well. The results reveal that the experimental and simulated electrical efficiencies of PV/T panels are 11.5% and 12.6%, respectively. The experimental and simulated thermal efficiencies of thermal collectors are 46.8% and 48.0%, respectively. The experimental and simulated final water temperatures in the tank are 59.3 °C and 60.9 °C, respectively. Based on these results, an error analysis is carried out. The experimental and simulation results of the system in summer provide a fundamental data and method for predicting

the annual performance of the system in the future.

Keywords: Mini-channel, PV/T, thermal collector, hot water, efficiency

NOMENCLATURE

A	Area, m^2
C_p	Specific heat at constant pressure, $Jkg^{-1}K^{-1}$
D	Hydraulic diameter,
d	Thickness, m
E_{pv}	Power output of PV layer, Wm^{-2}
G	Solar radiation, Wm^{-2}
k	Thermal conductivity, $Wm^{-1}K^{-1}$
l	Thickness of the air gap, m
M_w	Quality of water in the tank, kg
$\dot{m}_{wf}$	Mass flow rate of working fluid, kgs^{-1}
Nu	Nusselt number,
Pr	Prandtl number,
R	Thermal resistance, KW^{-1}
Ra	Rayleigh number,
Re	Reynolds number,

T Temperature, K

U Heat transfer co-efficient, $Wm^{-2}K^{-1}$

u_{wd} Wind speed, ms^{-1}

α Absorptivity,

β Angle of inclination of the plane with the horizontal,

σ Stefan-Boltzmann's constant,

τ_g Glass transmissivity,

ε Emissivity,

η Efficiency,

ρ Density, kg/m^3

Subscripts

air Air,

am Ambient,

am_gc Glass cover and ambient,

b Absorber plate,

b_am Absorber plate and ambient,

p_b Absorber plate and mini-channel tube,

b_gc Absorber plate and glass cover,

e Electricity,

gc Glass cover,

hcg Heat-conducting glue,

pv_gc Glass cover and PV layer,

mc Mini-channel tube,

Pwf Mini-channel tube and working fluid,

pv PV layer,

b_pv PV layer and absorber plate,

pvt PV/T panel，

rc Standard condition,

s Sky,

tk Storage tank,

$tk.i$ Inlet of storage tank,

$tk.o$ Outlet of storage tank,

$t.th$ Thermal energy of thermal collector,

th Thermal collector,

$th.i$ Inlet of thermal collector,

$th.o$ Outlet of thermal collector,

w Water,

wd Wind,

wf Working fluid,

1. Introduction

Global energy consumption has increased steadily in past years (Tzeiranaki et al., 2018; Bertoldi et al., 2013). The high living level, i.e., lighting, cooling and heating, has translated to increase in the energy consumption of building. In 2016, the residential energy consumption accounted for 25.71% of the EU's final energy consumption (Tzeiranaki et al., 2013). In China, it accounted for 20.6% of the total energy consumption (China Building Energy Research Report 2018). For the energy consumption in building, space heating and hot water takes the largest share, using 78% and 15% of the total residential energy usage in EU (EUROPEAN COMMISSION 2016), and space heating and hot water supply contribute 68% of energy consumption in China (Zheng et al., 2014). Therefore, it is very important to develop renewable energy system to replace the fossil energy consumption for reducing CO_2 emission and improving the environment.

Solar energy is a type of green and free renewable energy, which can be collected by PV panel, thermal collector and PV/T panel. These panels can be integrated to the building easily, therefore, it is a good way to combine solar energy panels to building for supplying electricity and thermal energy. Thermal collector is the most investigated technology to translate solar energy into thermal energy for generating hot water (Goswami et al., 2015). It can be cooled by air (Khanlari et al., 2020; Ural et al., 2019), water (Araya et al., 2017; Hajabdollahi et al., 2017), nanofluid (Eltaweel et al., 2019; Noghrehabadi et al., 2016), heat pipe (Zhang et al., 2017; Allouhi et al., 2019) and refrigerant (Aziz et al., 1999; Sun et al., 2014). K. Balaji et al. (Balaji et al., 2017) constructed a solar collector hot water system using heat transfer enhancer in absorber tube. It was found that the rod heat transfer enhancer provides higher heat transfer with a small increase in pumping power than tube heat transfer enhancer and plain tube flat plate solar collector. Edalatpour et al. (Edalatpour et al., 2017) investigated the thermal-hydraulic characteristics and exergy performance of tube-on-sheet flat plate solar collector using different working fluid. Col et al. (Col et al., 2013) compared the thermal performance of flat plate solar collectors with sheet-and-tube and roll-bond absorbers, and the result revealed that the roll-bond absorber has a much higher thermal efficiency.

PV/T is a device which combines PV panel and thermal collector together, and it can provide power and thermal energy at the same time (Kaushik et al., 2012; Joshi et al., 2018). It is an improved product based on PV panel and thermal collector, therefore, the coolant is the same as the thermal collector (Sarhaddi et al., 2010; Chow et al., 2007; Sardarabadi et al., 2017; Pei et al., 2011; Zhou et al., 2016). Zondag et al. (Zondag et al., 2003) experimentally investigated a sheet and tube PVT collector, and the result indicated that its daily thermal and electrical efficiency were 58% and 8.9%. Pang et al. (Pang et al., 2019) experimentally and theoretically studied a roll-bond PV/T hot water system, and the daily electrical, thermal and exergy efficiency of the PVT system were 13.67%, 40.56% and 15.56%. Chow et al. (Chow et al., 2006) tested a flat-box PV/T hot water system, and the results revealed that the electrical efficiency ranged from 10.7% to 12.3%, and thermal efficiency ranged from 39.0% to 48.6%.

Currently, both the PV/T panel and thermal collector use copper tube or flat-box as the heat exchanger to transfer solar energy. These tubes have a big cross section and hydraulic diameter, which decreases the Reynolds number and heat exchanger co-efficient of working fluid. To improve the heat transfer rate and overall efficiency of PV/T panel and thermal collector, mini-channel tube is chosen to replace the conventional heat exchanger. Mini-channel tube is a new type of heat exchanger, and it has a small hydraulic diameter (1mm < D_h < 6mm) (Dixit et al., 2015). The reduced equivalent diameter of the micro-channel can enhance its heat transfer rate under the same flow rate (Prajapati et al., 2016; Khan et al., 2014). In addition, the smooth surface of mini-channel tube has a bigger contact area with the absorber than copper tube.

Based on the benefit of mini-channel heat exchanger, a mini-channel PV/T panels and thermal collectors combined heat pump system is designed and constructed, which can provide thermal energy for space heating, generate electricity and hot water with a much higher energy efficiency. In this paper, the performance of this system in summer is tested for generating electricity and hot water. With the experimental data as the input parameters, a simulation model is developed and verified.

2. System setup

2.1 System description

As shown in **Fig. 1,** each of the 10 mini-channel PV/T panels and thermal collectors are connected in series, and then these two types of panels are connected in parallel, which can provide thermal energy and electricity for building. The testing room and water storage tank are connected in parallel and then linked to the solar panels system, which can consume and store thermal energy from solar panels. A water heat pump is set between the water storage and testing room, which can transfer thermal energy from storage tank to testing room in the night. For meeting different requirement of building in different seasons, this system has two operating modes, which are presented as follows:

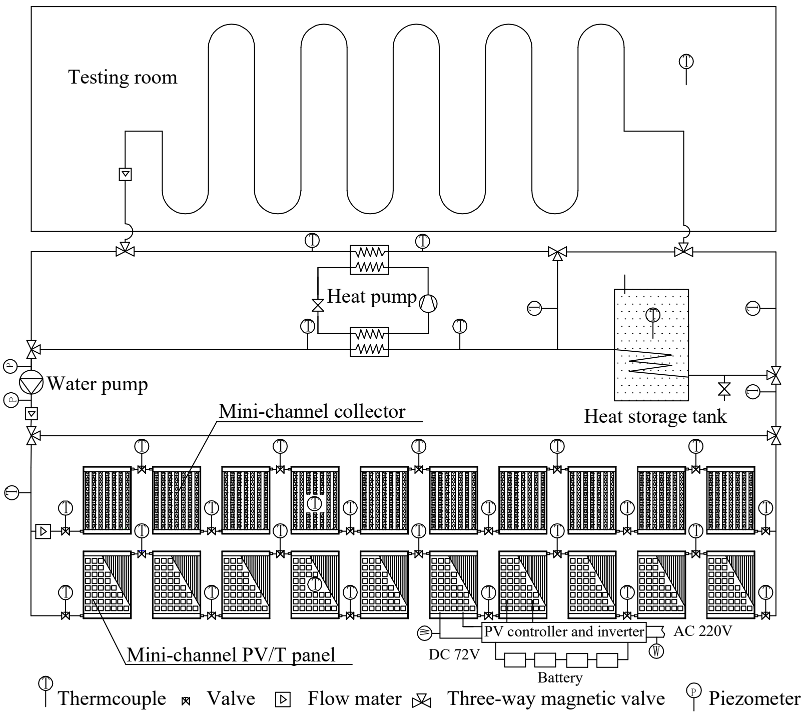

Fig. 1 Mini-channel PV/T panels and thermal collectors combined heat pump system (Zhou et al., 2017)

Space heating mode: In winter, when the system starts, the working fluid goes thorough mini-channel PV/T panels and thermal collector. If the solar radiation is weak and the thermal energy generated by the solar panels is not enough for space heating, the working fluid only enters the heat exchanger inside of the tank and releases energy to water. With the increase of solar radiation, if the temperature of working fluid at outlet of solar panels is higher than 40 ℃, the working fluid goes through storage tank and testing room at the same time. One part is for space heating, and the other is for storing surplus energy. In the night, the heat pump system starts and absorbs energy from storage tank and releases energy to testing room for space heating continually.

Hot water mode: In other seasons, this system can generate hot water and electricity for building. The working fluid goes through thermal collectors where it is heated, and then enters the heat exchanger inside of storage tank where the heat exchange takes place, releasing energy to water. The cooled working fluid goes back and enters thermal collectors again, completing a circulation. The air-vent at the back of mini-channel PV/T panel opens, and the air goes through it and cools the PV cell naturally.

2.2 System components

Mini-channel PV/T

To improve the annual electricity output, mini-channel PV/T panel is designed to be an unglazed type (**Fig. 2**) which consist a standard PV panel and a mini-channel layer. The constituent layers of this PVT collector are shown in **Fig. 3**. The size of PV/T panel is 1000 mm × 2000 mm. 72 pieces of polycrystalline silicon PV cells (size 156 mm × 156 mm) are connected in series and laminated on the glass. Its working voltage is 36 V, and maximum output power is 310 W, and electrical efficiency is 18% under standard condition. The mini-channel layer is composed of a piece of aluminium plate (size 1950 × 950 × 0.4 mm) and mini-channel heat exchanger, which are connected by thermally conductive glue. As shown in **Fig. 4**, nine mini-channel tube (**Fig. 5**) are welded into the two header pipes in parallel, and each of the header pipes is composed of two blind pipes, which work together to separate the nine mini-channel tubes to be three parts. An air vent is designed between the insulation and absorber plate, which can cool down the PV cell naturally in summer.

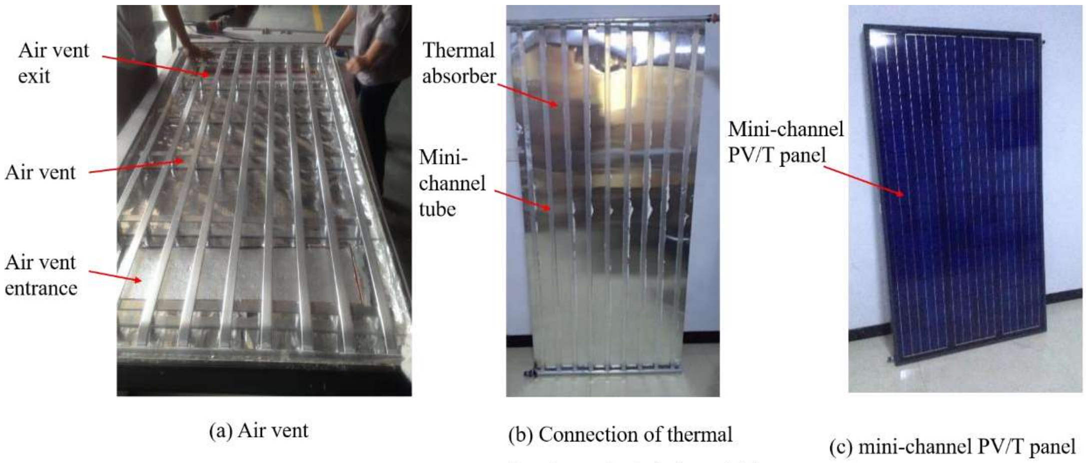

(a) Air vent (b) Connection of thermal absorber and mini-channel tube (c) mini-channel PV/T panel

Fig. 2 Mini-channel PV/T panel

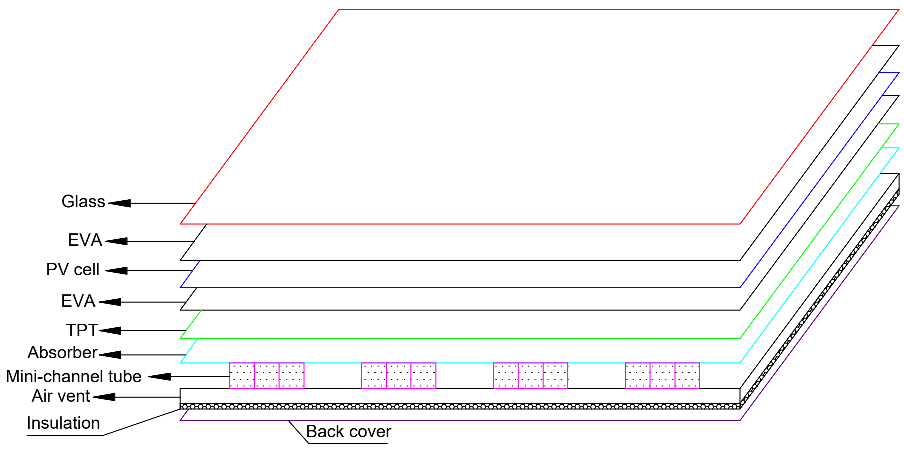

Fig. 3 Constituent layers of mini-channel PVT collector

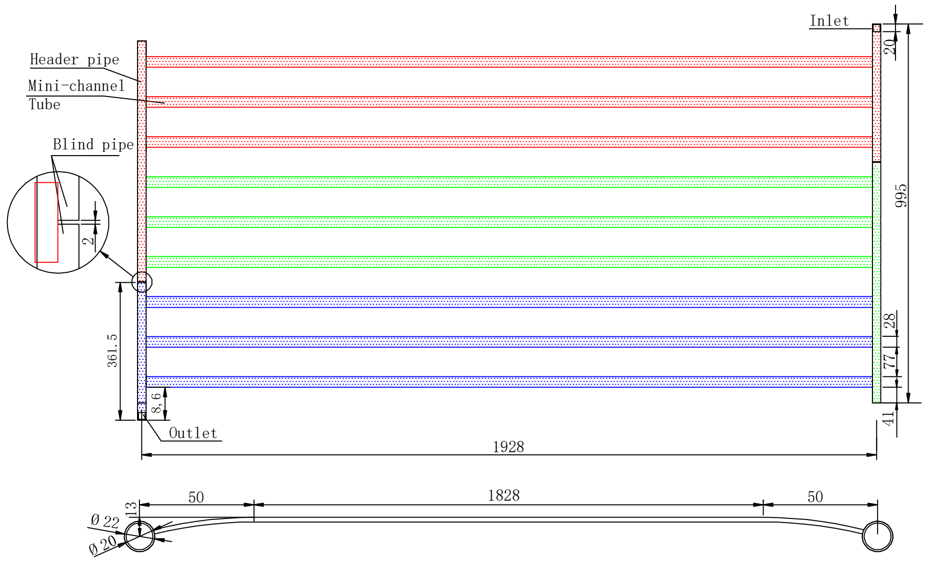

Fig. 4 Drawing of mini-channel layer

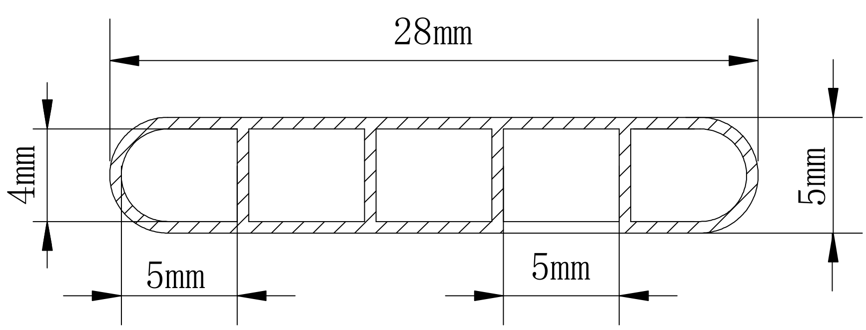

Fig. 5 Drawing of mini-channel tube

Mini-channel thermal collector

To improve the thermal energy generation, Mini-channel thermal collector is designed to be a glazed type, which has a similar structure as the PV/T panel, and the difference between them are that: 1) an air gap is designed between the glass cover and absorber; 2) PV cells are removed; 3) an absorber with black chrome replacing the aluminium plate in PV/T panel; 4) air vent is removed. Tts structure is shown in **Fig. 6 and Fig. 7**.

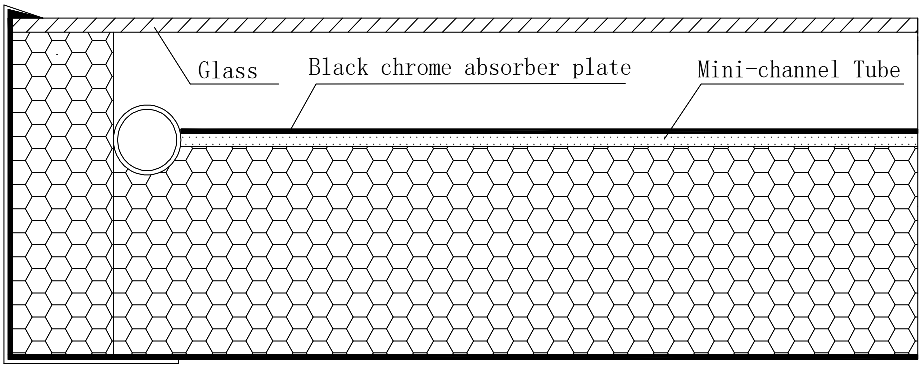

Fig. 6 Sectional view of the mini-channel solar thermal panel

Fig. 7 Mini-channel solar thermal panel

The sizes and material of each component is shown in **Table 1**. Several parameters in this system, i.e. temperature, flow rate, power output, current, etc., are tested and collected, and the technical properties of the measurement devices are given in **Table 2 (Zhou et al. 2017).**

Table 1 Sizes and description of the components

NO	Components	Size	Description
1	PV/T	2000*1000*80 mm	Effective area:1.85 m^2 Maximum output power : 310 W Electrical efficiency: 17%
2	Thermal panel	2000*1000*80 mm	Effective area:1.85m^2
3	Heat storage tank	1 m^3	Height:1180 mm Diameter:1190 mm Thickness of insulation: 50 mm
4	Coil-type-heat-exchanger	1.32 m^2	Quantity: 2 Diameter:15 mm Thickness:1 mm Length:14 m
5	Heat pump	880*660*1470 mm	Refrigerant: R-22 Cooling capacity: 9.9 KW Input power: 2.1 KW Heating capacity: 12 KW
6	Inverter	400*850*850 mm	Output power: 4 kW Input direct voltage: 24 V Output alternating voltage: 220 V
7	Water pump	12.6 kg	Max.lift head: 25 m Max Input power: 850 W Max flow rate: 115L/min

Table 2 Technical properties and uncertainties of the measurement devices

Devices	Specification	Property	Sensibility	Uncertainty	Location
Power sensor	HK-D4I CE-P03-32BS	0~2200 W	1%	±11W	In the room, Connected to the heat pump
Pyranometer	TQB-2	0~2000 W/m^2	7~14$\mu V/Wm^{-2}$	< ±2%	Top of panel
Water flowmeter	LWGY-C	0.5~10 m^3/h	-	±1%	Entrance of PV/T and thermal panels, exit of room, Entrance of PV/T

Current sensor	HK-14	0~10 A	±1%	-	In the room, connected to the PV/T panel
Thermocouple	T type	-200~+350 °C	±0.5 °C	±0.5 °C±0.1%*T	absorber of PV/T and thermal panel, Entrance and exit of PV/T, thermal panel, storage tank, testing room, evaporator and condenser of heat pump, ambient and room temperature.
Data logger	34970 A	20 channel	-	-	In the room
Pressure gauge	YN60	0-600 kpa	±1%	±6 kpa	Entrance and exit of water pump

3. Simulation model

3.1 Simulation model for mini-channel PV/T panel

The simulation model of mini-channel PV/T panel consists of glass cover, PV layer, absorber and mini-channel heat exchanger. And the heat transfer process is shown in **Fig. 8**.

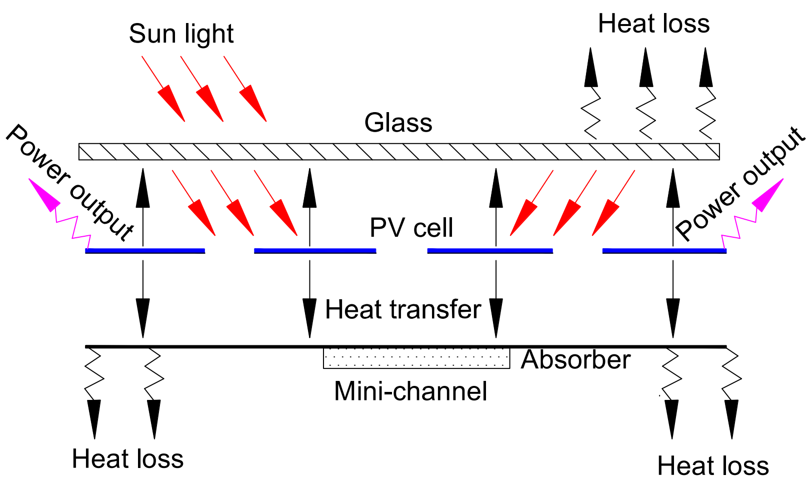

Fig. 8 Energy transfer process in mini-channel PV/T panel

For glass cover (Chow et al., 2006)

$$\mathrm{d}_{gc}\rho_{gc}\mathrm{C}_{p.gc}\frac{\partial T_{gc}}{\partial t} = G\lambda_{gc} + \alpha_{pv\_gc}\left(T_{gc} - T_{pv}\right) - \alpha_{am\_gc}\left(T_{gc} - T_{am}\right) \quad (1)$$

$$\alpha_{am\_gc} = 2.8 + 3.0u_{wd} \quad (2)$$

where, d_{gc} is the thickness of the glass cover (m); ρ_{gc} is the density of glass cover (kg/m^3); $C_{p.gc}$ is the specific heat capacity of glass cover (J/(kg·K)); T_{gc} is the temperature of the glass cover (K); T_{am} is the ambient temperature (K); α_{am_gc} and α_{pv_gc} is the heat transfer co-efficient between the glass cover and the ambient air and PV cell respectively (W/(m^2·K)); S_{wd} is the wind speed (m/s); u_{wd} is the wind speed (ms^{-1}).

For PV layer (Chow et al., 2006)

$$\zeta d_{pv}\rho_{pv}C_{p.pv}\frac{\partial T_{pv}}{\partial t} = G(\tau\alpha)_{pv} - \frac{T_{pv}-T_b}{R_{b\_pv}} - \alpha_{pv\_gc}\left(T_{pv} - T_{gc}\right) - E_{pv} \quad (3)$$

$$E_{pv} = \alpha_{pv}\tau_g G A_{pv}\eta_{rc}[1 - 0.0045\left(T_{pv} - T_{rc}\right)] \quad (4)$$

Where, ζ is coverage factor of PV cell; d_{pv} is the thickness of the PV cell (m); ρ_{pv} is the density of PV cell (kg/m^3); $C_{p.pv}$ is the specific heat capacity of PV cell (J/(kg·K)); α_{pv} is PV absorptivity; τ_g is Glass transmissivity; T_b is the temperature of absorber plate (K); R_{b_pv} is the thermal resistance between PV layer and aluminium plate (K·m^2/W). E_{pv} is the power output of PV layer (Wm^{-2}); η_{rc} is the electrical efficiency of PV under standard condition (18%); T_{rc} is the reference operating temperature (298.15 K).

For absorber plate (Chow et al., 2006)

$$\rho_b c_{p.b} \frac{\partial T_b}{\partial t} = K_b \frac{\partial^2 T_b}{\partial y^2} + \frac{1}{d_b} [\frac{T_{am} - T_b}{R_{b\_am}} + \frac{T_{pv} - T_b}{R_{b\_pv}}] \quad (5)$$

$$R_{b\_am} = \frac{l}{k_{air} Nu} \quad (6)$$

$$Nu = 1 + 1.14 \left(1 - \frac{1708 \times (\sin 1.8\beta)^{1.6}}{Ra \times \cos\beta}\right) [1 - \frac{1708}{Ra \cos\beta}]^{+} + [(\frac{Ra \times \cos\beta}{5830})^{1/3} - 1]^{+} \quad (7)$$

Where, ρ_b, $C_{p.b}$, d_b, T_b and K_b are the density (kg/m^3), specific heat capacity (J/(kg·K)), thickness (m), temperature (K) and thermal conductivity (W/(m·K)) of the aluminium plate, respectively; R_{b_am} and R_{b_pv} is the thermal resistance between the aluminium plate and surrounding, aluminium plate and PV layer (K/W). Nu is the Nusselt number of the air between the insulation and absorber; β is the angle of inclination of the plane with the horizontal; Ra is the Rayleigh number. + presents that if the figure in the$[\quad]^{+} > 0$, then keep on, if not, the figure will be set at 0.

3.2 Mini-channel thermal collector

The simulation models of mini-channel thermal collector are composed of glass cover, absorber plate, mini-channel heat exchanger and working fluid. They have a similar energy transfer process and equations as the PV/T panel. The energy transfer process is shown in **Fig. 9**, and the differences are as follows:

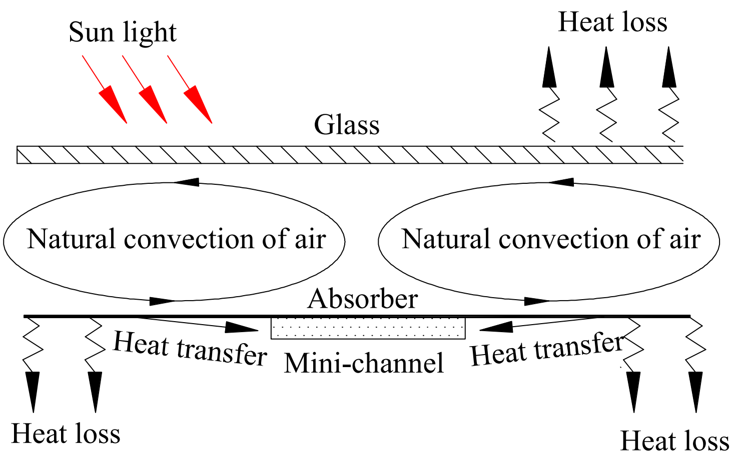

Fig. 9 Energy transfer process in mini-channel thermal panel

For glass cover (Chow et al., 2006)

$$d_{gc}\rho_{gc}c_{p.gc}\frac{\partial T_{gc}}{\partial t} = G\lambda_{gc} + \alpha_{b\_gc}\left(T_{gc} - T_b\right) - \alpha_{am\_gc}\left(T_{gc} - T_{am}\right) \qquad (8)$$

$$\alpha_{b\_gc} = \sigma({T_b}^2 + {T_{gc}}^2)(T_b + T_{gc})\frac{1}{\frac{1}{\varepsilon_b}+\frac{1}{\varepsilon_{gc}}-1} + \frac{Nu{\cdot}k_{air}}{l} \qquad (9)$$

Where, α_{b_gc} is the heat transfer coefficient between the glass cover and absorber (W/(m^2·K)); ε_b and ε_{gc} is the emissivity of the absorber and glass cover, respectively.

For absorber plate (Chow et al., 2006)

The absorber plate are divided into two parts: (1) the first part which connects the mini-channel directly; (2) the second part which acts as the fin. Their models are given as follows:

The equation of the first part can be expressed as:

$$\rho_b c_{p.b}\frac{\partial T_b}{\partial t} = K_b\frac{\partial^2 T_b}{\partial y^2} + \frac{1}{d_b}\left[G(\tau\alpha)_b - \frac{T_b - T_{am}}{R_{b\_am}} - \frac{T_b - T_{gc}}{R_{b\_gc}} - \frac{T_b - T_p}{R_{p\_b}A_{bi}}\right] \qquad (10)$$

The equation of the second part can be expressed as (Chow et al., 2006):

$$\rho_b c_{p.b}\frac{\partial T_b}{\partial t} = \lambda_b\frac{\partial^2 T_b}{\partial y^2} + \frac{1}{d_b}\left[G(\tau\alpha)_b - \frac{T_b - T_{am}}{R_{b\_am}} - \frac{T_b - T_c}{R_{b\_c}}\right] \qquad (11)$$

Where, $(\tau\alpha)_b$ is the effective absorbance of the absorber plate. A_{bi} is the heat exchange area of the selected microelement (m^2), and its equation can be given as:

$$A_{bi} = W_b \times dy \tag{12}$$

Where, W_b is the length of the panel (m); dy is the width of the selected microelement (m).

$$R_{p\_b} = d_{hcg}/(K_{hcg}A_{p\_b}) \tag{13}$$

Where, d_{hcg} and K_{hcg} are the thickness (m) and thermal conductivity (W/(m·K)) of the heat-conducting glue, respectively; A_{p_b} is the contact area between the mini-channel tube and aluminium plate (m^2).

For mini-channel tube (Chow et al., 2006)

$$\rho_p c_{p.p}\frac{\partial T_p}{\partial t} = \mathrm{K}_p\frac{\partial^2 T_p}{\partial y^2} + \frac{1}{A_p}[\pi D_p \alpha_{pwf}(T_{wf} - T_p) + (T_b - T_p)/R_{p\_b}] \tag{14}$$

$$\alpha_{pwf} = 0.023\frac{{Re_{wf}}^{0.8}{Pr_{wf}}^{0.3}k_{wf}}{D_p} \tag{15}$$

where, ρ_p, $C_{p.p}$and K_b are the density (kg/m^3), specific heat capacity (J/(kg·K)) and thermal conductivity (W/(m·K)) of the micro-channel tube, respectively; A_p is the cross section area of the micro-channel tube; D_p is the hydraulic diameter of mini-channel (m); α_{pwf} is heat transfer co-efficient between mini-channel tube and working fluid (Wm^{-2}K^{-1}); T_{wf} is the temperature of working fluid (K);

For working fluid (Chow et al., 2006)

$$(mc_p)_{wf}\frac{\partial T_{wf}}{\partial t} = (T_p - T_{wf})/R_{pwf} \tag{16}$$

where, m is mass flow of working fluid in one calculation unit (kg); R_{pwf} is the thermal resistance between the micro-channel tube and working fluid (K/W).

3.3 Simulation model for water in the storage tank

The water in the tank is used for storing the thermal energy from the solar panels, and its equation can be expressed as (Chow et al., 2006):

$$M_w C_{p.w} \Delta T = \dot{m_{wf}} C_{p.wf} (T_{tk.i} - T_{tk.o}) + \alpha_{wam} A_{tk} (T_{am} - T_w) \quad (17)$$

where, M_w is the quality of water in the tank (kg); $\dot{m_{wf}}$ is mass flow rate of working fluid in the tank (kgs^{-1}); α_{wam} is the heat transfer co-efficient between water and ambient (Wm^{-2}K^{-1}); A_{tk} is the outside surface of tank (m^2); $T_{tk.i}$, $T_{tk.o}$ and T_w are the inlet, outlet temperature of tank and water temperature in the tank (K).

3.4 Performance of the system

The electrical efficiency of the PV/T panels is given by (Zhou et al., 2017):

$$\eta_e = \frac{E_{pv}}{G A_{pvt}} \quad (18)$$

The thermal efficiency of the panels can be expressed as (Zhou et al., 2017):

$$\eta_{t.th} = \frac{C_{p.wf} \dot{m_{wf}} (T_{th.o} - T_{th.i})}{G A_{th}} \quad (19)$$

Where A_{th} is the total effective area of thermal collector (m^2); $T_{th.i}$ and $T_{th.o}$ are the temperatures at the inlet of the first thermal panel and the outlet of the last thermal panel (K), respectively.

3.5 Model set-up and operational procedure

The equations of components of mini-channel PV/T panel, thermal collector and water storage tank are developed. The iterative calculation of the above equations is solved by the computer language C. The calculation flow chart is shown in **Fig. 10** and the calculation steps are as follows:

1) Start the program, and initialize the parameters of the mini-channel PV/T and thermal panel;
2) Input the weather parameters (solar radiation, ambient temperature, etc.), and input the parameters at the inlet of the panels, including the temperature, mass flow rate and specific enthalpy of the working fluid;
3) Solve the equation of the glass cover of PV/T panel, and calculate the temperature of glass cover T_{gc};
4) Solve the equation of PV layer based on the glass cover temperature T_{gc}, and calculate the temperature of the PV layer T_{pv} and output power of the PV/T panel E_{pv};
5) Solve the equation of the aluminium plate based on the temperature of PV layer T_{pv} and ambient temperature T_{am}, and calculate the temperature of absorber T_b;
6) Solve the equation of the glass cover of thermal collector, and calculate the temperature of glass cover T_{gc};
7) Solve the equation of the absorber and mini-channel tube of thermal collector, and calculate its temperature T_b and T_p;
8) Solve the equation of the working fluid; calculate the temperature at outlet of thermal panel $T_{th.o}$;
9) Solve the equation of the storage tank, calculate the temperature of the water T_w;

10) Solve the equation of the working fluid; calculate the temperature at outlet of tank $T_{tk.o}$;

11) Check if the calculated value of each parameter has reached the calculation accuracy ($|T_{sim} - T_{set}|/T_{set} < 10^{-3}$, computation time 480 minutes) If no, return to step 3) and continue iterative solution; if yes, then output the results;

12) End the calculation program.

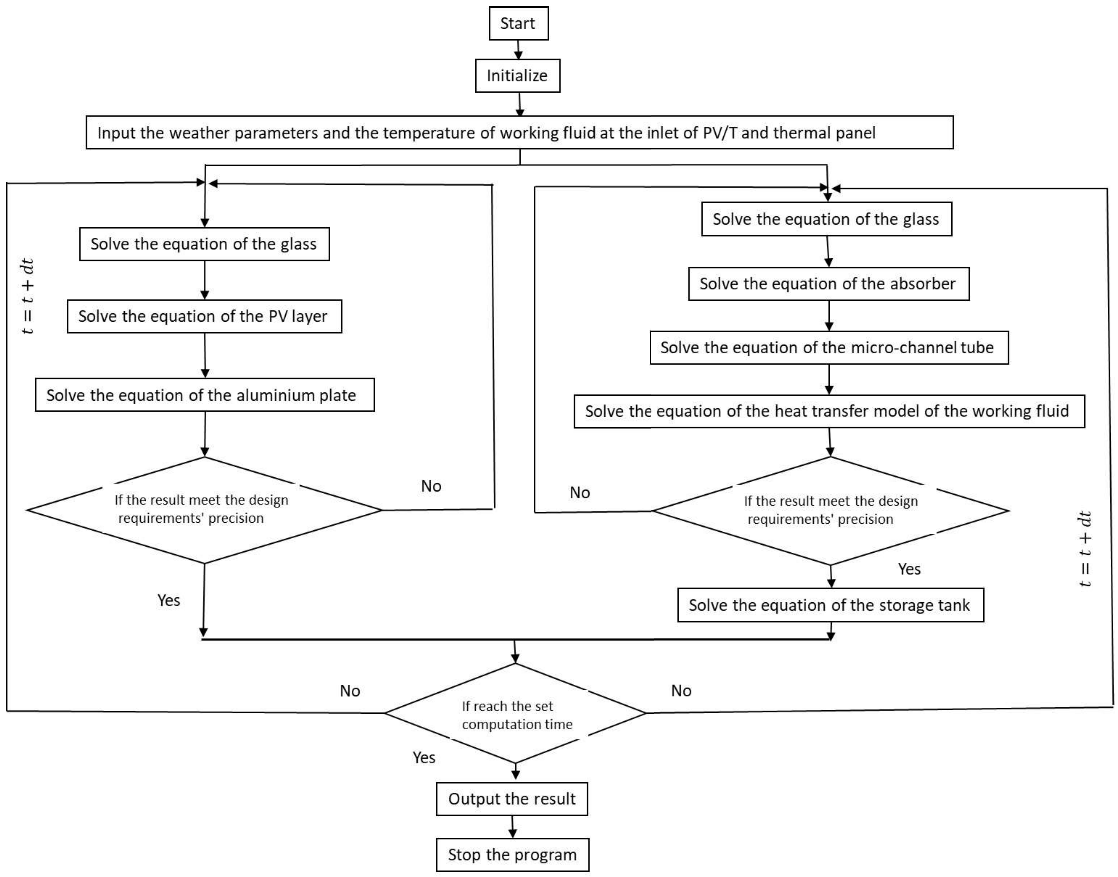

Fig. 10 Calculation flow chart of mini-channel PV/T and thermal collector hot water system

4 Experimental performance of the system in summer

The performances of this system in winter under the clear days and low solar radiation condition have been tested (Zhou et al., 2017; Zhou et al., 2020). In this paper, the performance of this system for generating hot water in summer is presented. The experiment is carried out from 21th to 27th July 2016. The testing result is shown in **Table 3**, and a typical day's weather data is chosen as the input parameters to verify the simulation model. The experimental and simulated results are compared.

Table 3 Testing result of the system in summer

Date	Radiation(W/m2)	Temperature ℃			System performance (%)	
2016	G	T_a	T_{wt}^i	T_{wt}^f	$\eta_{t.Th}$	$\eta_{e.PVT}$
21/07	685.6	13.2	22.2	56.1	45.6	11.9
22/07	703.4	12.8	22.7	57.4	46.2	11.5
23/07	697.5	11.1	23.1	56.9	45.8	11.8
24/07	736.4	9.1	22.9	57.8	44.9	12.0
25/07	743.8	8.4	22.5	58.6	47.0	11.0
26/07	723.6	8.7	21.6	56.9	46.3	11.2
27/07	765.5	6.4	23.2	59.3	46.8	11.5

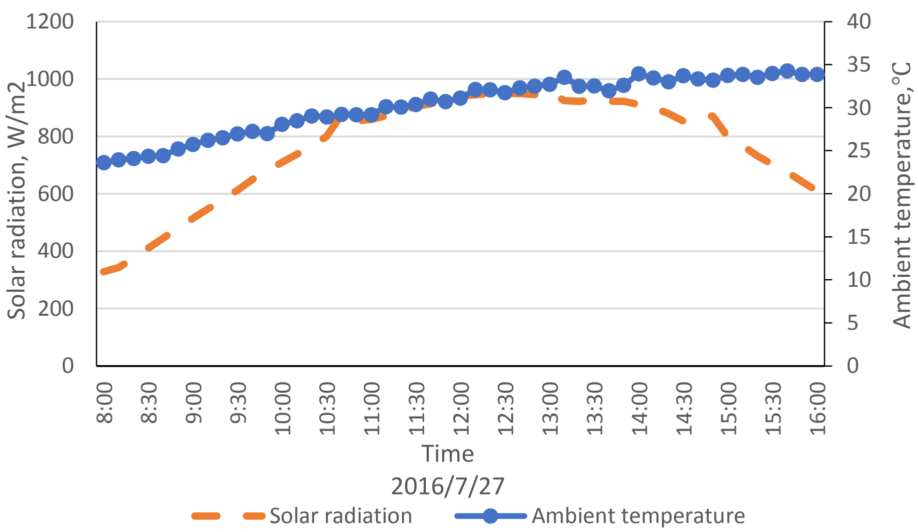

Fig. 11 Variation of the solar radiation and ambient temperature in a sunny day

Fig. 11 displays the solar radiation and ambient temperature. The ambient tempature increases with time and reaches a stable value at noon (from 23.5 ºC to 33.5 ºC during 8:00 to 13:10), and then keeps steady (33.8 ºC) in the afternoon. The variation trend of the solar radiation is a parabolic curve, which increases from 330 W/m^2 to 950 W/m^2 (8:00 - 12:40), and then drops to 610 W/m^2 (12:40 - 16:00).

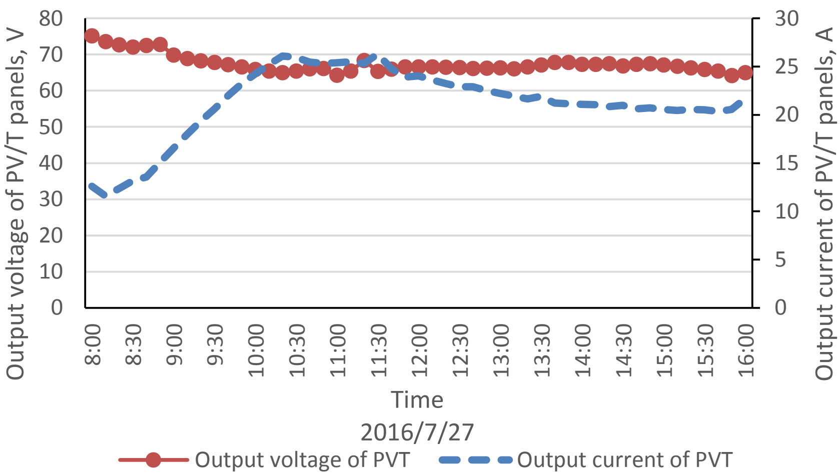

Fig. 12 Output voltage and current of the PV/T panels in sunny day

Fig. 12 shows the output voltage and current of the PV/T panels. The output voltage of the PV/T panel remains at 68 V, while the output current increased from 11.5 A to 26 A, and then dropped to 20 A during the testing time. The output current was not only impacted by the solar radiation, but also the inverter. The inverter can show a good performance when the voltage of battery is between 46 V to 52 V. However, the power of the electrical load was stable, while the input power is changing all times, therefore, the output current does not match the solar radiation very well sometimes.

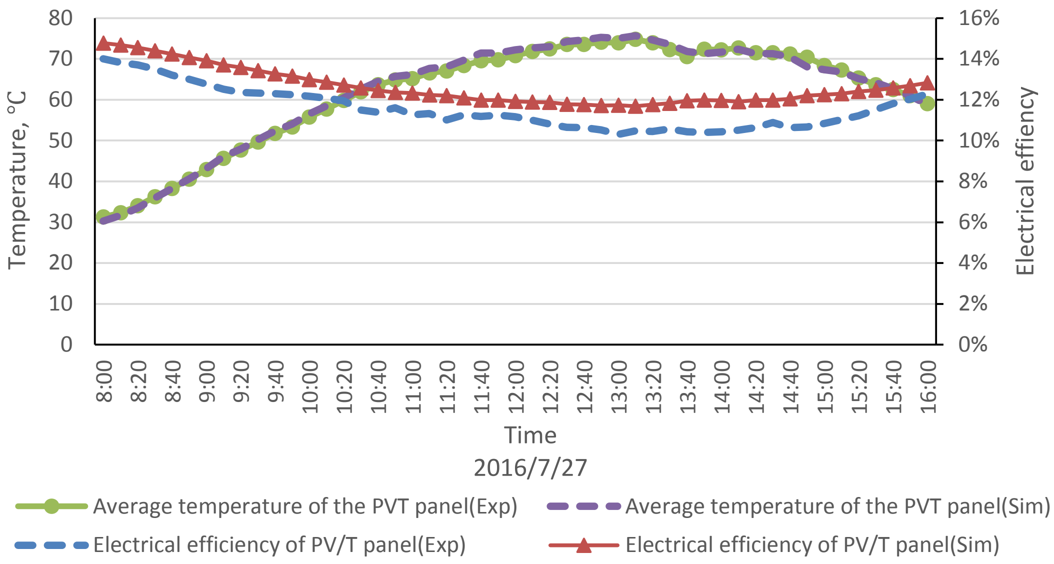

Fig. 13 Experimental and simulated absorber temperature and electrical efficiency of PV/T panels

Fig. 13 shows the variation of experimental and simulated absorber temperature and electrical efficiency of PV/T panels. With a natural convection cooling by the surrounding air, the surface temperature of PV/T panel is affected by the solar radiation. It shows a similar trend as solar radiation, which rises from 30 ºC to 75 ºC in the morning and then drops to 59 ºC in the afternoon. The electrical efficiency shows an opposite trend as the solar radiation, because it is affected by the operating temperature, a high operating temperature with a lower electrical efficiency. The electrical efficiency ranges from 10.4% to 14.7%, and the average experimental and simulated electrical efficiency are 11.5% and 12.6%, respectively.

Fig. 14 shows the experimental and simulated inlet and outlet temperature of thermal collectors. These two temperatures are not only affected by the solar radiation but also by the water temperature in storage tank (**Fig. 16**). With the increase of water temperature in the tank, the inlet temperature increases from 26 ºC to 64 ºC, while the outlet temperature increases from 30 ºC to 77 ºC and then drops to 71 ºC. The temperature difference between the inlet and outlet ranges from 3 ºC to 15 ºC, and it increases from 8:00 to 13:00, then decreases in the afternoon. The flow rate of working fluid remains at 0.56 m^3/h.

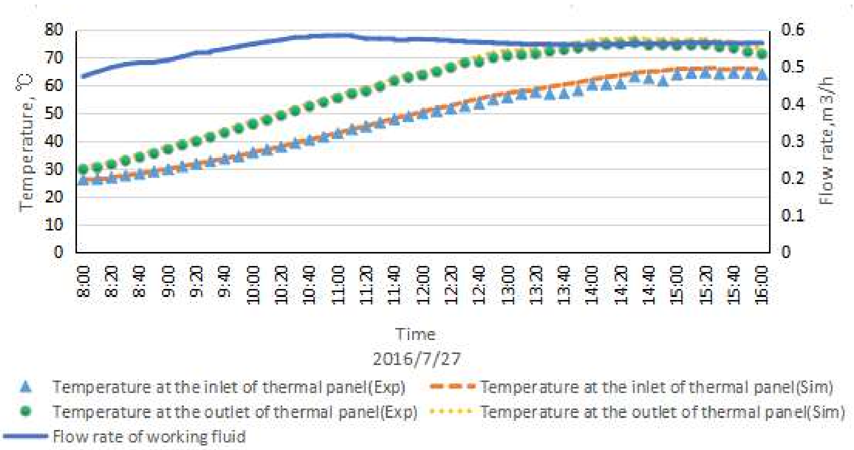

Fig. 14 Experimental and simulated inlet, outlet temperature of thermal collector and flow rate of working fluid in it

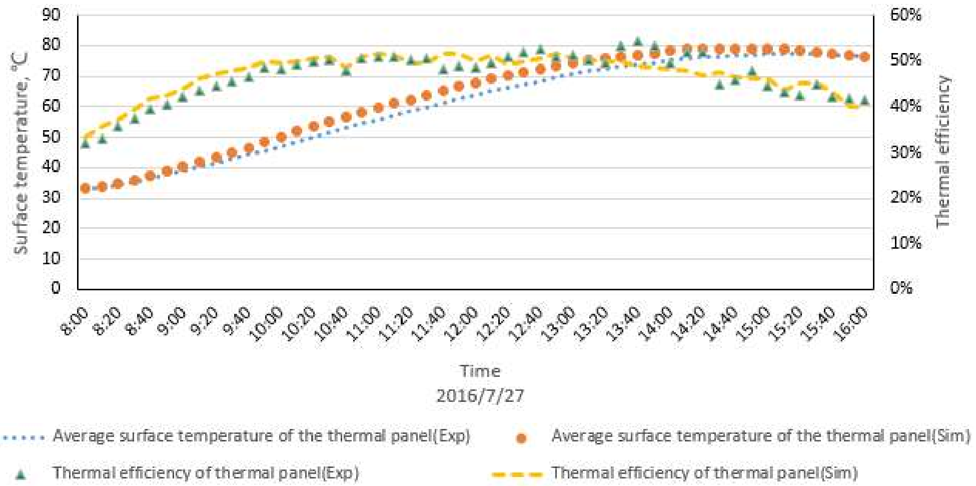

Fig. 15 Experimental and simulated absorber temperature and thermal efficiency of thermal collector

Similarly, the absorber temperature of thermal collectors (**Fig. 15**) is affected by the solar radiation and inlet temperature of working fluid, and it shows a similar variation trend as the inlet and outlet temperature of thermal collectors. It increases from 33 ºC to 79 ºC and then decreases to 76 ºC. The thermal efficiency is affected by the solar radiation and temperature difference between the inlet and outlet of thermal panel, and has a similar variation trend as them. It rises from 31.9% to 51.2% in the morning and then drops to 41.4% in the afternoon. The thermal efficiency ranges from 33.5% to 51.6%, and the experimental and simulated daily average thermal efficiency are 46.8% and 47.0%, respectively.

Fig. 16 shows the variation of experimental and simulated water temperature in storage tank. With the hot working fluid releasing thermal energy to the water continually, the water temperature rises from 23 ºC to 59 ºC. The temperature variation speed is affected by the solar radiation and thermal efficiency. When the solar radiation is not strong (below 600 W/m^2) and a low thermal efficiency, the water temperature rises very slowly (4 ºC in 2 hours), while when the solar radiation is high (over 600 W/m^2) and high thermal efficiency, it rises very quickly (32 ºC in 6 hours).

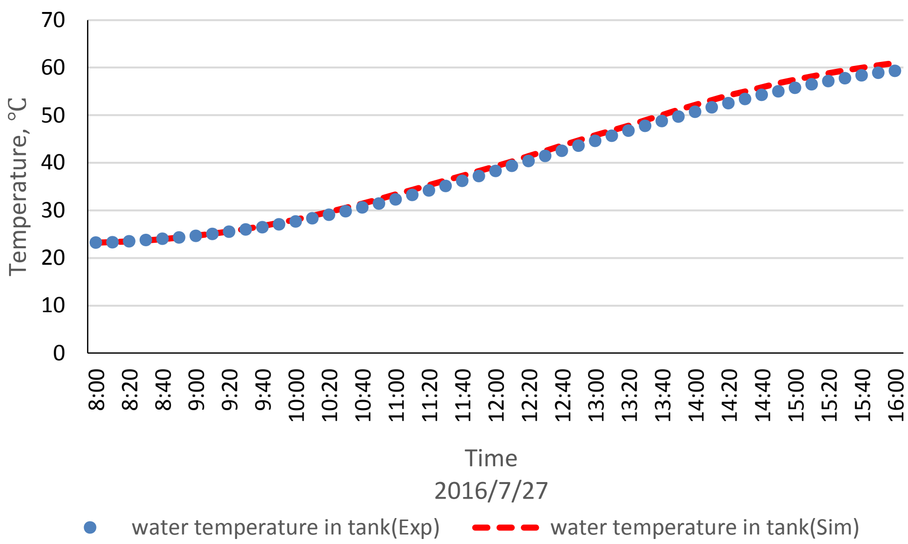

Fig. 16 Experimental and simulated water temperature in storage tank

4.1 Simulated VS experimental data analysis

It can be found that most of the most significant results agreed with each other very well, and their error are shown in the **Table 4**. The high error of the performance efficiency is caused by several reasons, i.e., testing error, unstable practical operating condition. The electrical efficiency is impacted by the inverter and load, and the other efficiency is calculation value and affected by the measurement errors.

Table 4 Average error of the system and performance

	PVT		Thermal collector				Tank
	T_b (°C)	η_e	T_b (°C)	$T_{th.i}$ (°C)	$T_{th.o}$ (°C)	η_{th}	T_w (°C)
Excremental result	61.7	12.6%	60.4	47.7	58.9	46.8%	59.3
Simulated result	62.0	11.5%	62.9	48.7	60.4	47.0%	60.9
Error	5%	9.3%	4.2%	2.0%	2.4%	5.4%	2.7%

5 Conclusion

In this paper, a mini-channel PV/T and thermal collector hot water system is presented. The novel PV/T panel and thermal collector use mini-channel tube as the heat exchanger, which has a small hydraulic diameter and large heat exchanger area, to enhance the heat transfer coefficient of working fluid, resulting in a higher electrical and thermal efficiency. This system is designed, constructed and tested at the selected clear days of Lvliang city, China.

The testing for generating hot water in summer is carried out, and an integral simulation model is developed. One typical day's weather data is selected as the input parameters to verify the simulation model. The experimental and simulated electrical efficiency of PV/T panels are 11.5% and 12.6%, respectively. The inlet temperature of thermal panel is related to the water temperature in the tank, and it increases first and remains steady. The outlet temperature and surface temperature are affected by the inlet temperature and solar radiation, and they show a rising trend first and a light decrease. The experimental and simulated thermal efficiency of thermal collectors are 46.8% and 48.0%, respectively. The experimental and simulated finial water temperatures in the tank are 59.3 ºC and 60.9 ºC, respectively. The errors of these data are analyzed, and the electrical efficiency has the maximum value of 9.3%, while inlet temperature of thermal collector has the minimum value of 2.0%.

The experimental and simulation results of the system in summer provided fundamental data and method for the performance analysis of whole year and improvement of similar system in the future.

Acknowledgement

The work of this paper was sponsored by Shanxijingxu renewable energy Co. Ltd, China.

Reference

A. Allouhi, M. Benzakour Amine, M.S. Buker, T. Kousksou, A. Jamil. Forced-circulation solar water heating system using heat pipe-flat plate collectors: Energy and exergy analysis. Energy 180 (2019) 429-443.

Aminreza Noghrehabadi, Ebrahim Hajidavalloo, MojtabaMoravej. Experimental investigation of efficiency of square flat-plate solar collector using SiO_2/water nanofluid. Case Studies in Thermal Engineering 8 (2016) 378-386.

Ataollah Khanlari, Hande €Ozge Güler, Azim Dogus Tuncer, Ceylin S irin,Yasar Can Bilge, Yusuf Yılmaz, Afsin Güngor. Experimental and numerical study of the effect of integrating plusshaped perforated baffles to solar air collector in drying application. Renewable Energy 145 (2020) 1677-1692.

Bertoldi, P. Hirl, B. An econometric model to access residential electricity savings in the EU. In Proceedings of the 7th International Conference EEDAL 2013 Energy Efficiency in Domestic Appliances and Lighting, Coimbra, Portugal, 11-13 September 2013.

China Building Energy Research Report (2018), China association of building energy efficiency, Shanghai, 2018.11.12.

Davide Del Col, Andrea Padovan, Matteo Bortolato, Marco Dai Prè, Enrico Zambolin. Thermal performance of flat plate solar collectors with sheet-and-tube and roll-bond absorbers. Energy 58 (2013) 258-269.

Dongwei Zhang, Hanzhong Tao, Mimi Wang, Zishuai Sun, Chuan Jiang. Numerical simulation investigation on thermal performance of heat pipe flat-plate solar collector. Applied Thermal Engineering 118 (2017) 113-126.

F. Sarhaddi, S. Farahat, H. Ajam, A. Behzadmehr, M. Mahdavi Adeli. An improved thermal and electrical model for a solar photovoltaic thermal (PV/T) air collector. Applied Energy 87 (2010) 2328-2339.

H.A. Zondag, D.W. de Vries, W.G.J. van Helden, R.J.C. van Zolingen, A.A. van Steenhoven.The yield of different combined PV-thermal collector designs. Solar Energy 74 (2003) 253-269.

Jinzhi Zhou, Xudong Zhao, Xiaoli Ma, Zhongzhu Qiu, Jie Ji, Zhenyu Du, Min Yu. Experimental investigation of a solar driven direct-expansion heat pump system employing the novel PV/micro-channels-evaporator modules. Applied Energy 178 (2016) 484-495.

Jinzhi Zhou, Xudong Zhao, Xiaoli Ma, Yi Fan. Clear-days operational performance of a hybrid experimental space heating system employing the novel mini-channel solar thermal & PV/T panels and a heat pump. Solar Energy 155 (2017) 464-477.

Jinzhi Zhou, Xiaoli Ma, Xudong Zhao, Yanping Yuan, Min Yu, Jing Li. Numerical simulation and experimental validation of a micro-channel PV/T modules based direct-expansion solar heat pump system. Renewable Energy 145 (2020) 1992-2004.

Jinzhi Zhou, Xudong Zhao, Yanping Yuan, Jing Li, Min Yu, Yi Fan. Operational performance of a novel heat pump coupled with mini-channel PV/T and thermal panel in low solar radiation, Energy and Built Environment, https://doi.org/10.1016/j.enbenv.2019.08.001.

K. Balaji, S. Iniyan, V. Muthusamyswami. Experimental investigation on heat transfer and pumping power of forced circulation flat plate solar collector using heat transfer enhancer in absorber tube. Applied Thermal Engineering 112 (2017) 237-247.

Khan JA, Monjur Morshed AKMM, Fang R. Towards ultra-compact high heat flux micro-channel heat sink. Procedia Eng 90 (2014) 11-24.

Mahmoud Eltaweel, Ahmed A. Abdel-Rehim. Energy and exergy analysis of a thermosiphon and forcedcirculation flat-plate solar collector using MWCNT/Water Nanofluid. Case Studies in Thermal Engineering 14 (2019) 100416.

Mojtaba Edalatpour, Juan P. Solano. Thermal-hydraulic characteristics and exergy performance in tube-on-sheet flat plate solar collectors: Effects of nanofluids and mixed convection. International Journal of Thermal Sciences 118 (2017) 397-409.

Mohammad Sardarabadi, Mohammad Hosseinzadeh, Arash Kazemian, Mohammad Passandideh-Fard. Experimental investigation of the effects of using metaloxides/water nanofluids on a photovoltaic thermal system (PVT) from energy and exergy viewpoints. Energy 138 (2017) 682-695.

Pei Gang, Fu Huide, Zhang Tao, Ji Jie. A numerical and experimental study on a heat pipe PV/T system. Solar Energy 85 (2011) 911-921.

Prajapati YK, Pathak M, Khan MK. Transient heat transfer characteristic of segmented finned micro-channels. Exp Therm Fluid Sci, 79 (2016) 134-142.

R. Araya, F. Bustos, J. Contreras, A. Fuentes.Life-cycle savings for a flat-plate solar water collector plant in Chile. Renewable Energy 112 (2017) 365-377.

R. Nasrin, N.A. Rahim, H. Fayaz, M. Hasanuzzaman, Water/MWCNT nanofluid based cooling system of PVT: experimental and numerical research, Renew. Energy 121 (2018) 286-300.

Sandeep S. Joshi, Ashwinkumar S. Dhoble. Photovoltaic -Thermal systems (PVT): Technology review and future trends. Renewable and Sustainable Energy Reviews 92 (2018) 848-882.

Sofia Tsemekidi Tzeiranaki, Paolo Bertoldi, Francesca Diluiso, Luca Castellazzi, Marina Economidou, Nicola Labanca, Tiago Ribeiro Serrenho, Paolo Zangheri. Analysis of the EU Residential Energy Consumption: Trends and Determinants. Energies 2019, 12, 1065; doi:10.3390/en12061065.

Tisha Dixit, Indranil Ghosh. Review of micro-and mini-channel heat sinks and heat exchangers for single phase fluids. Renewable and Sustainable Energy Reviews 41 (2015) 1298-1311.

Tolga Ural. Experimental performance assessment of a new flat-plate solar air collector having textile fabric as absorber using energy and exergy analyses. Energy 188 (2019) 116116.

Tsemekidi-Tzeiranaki, S.; Bertoldi, P.; Labanca, N.; Castellezzi, L.; Serrenho, T.; Economidou, M.; Zangheri, P. Energy Consumption and Energy Efficiency Trends in the EU-28 for the Period 2000-2016; EUR 29473 EN; Publications Office of the European Union: Luxembourg, 2018.

T. T. Chow, J. Ji, W. He. Photovoltaic-Thermal Collector System for Domestic Application. Journal of Solar Energy Engineering, 129 (2007) 205-209.

T.T. Chow, W. He, J. Ji. Hybrid photovoltaic-thermosyphon water heating system for residential application. Solar Energy 80 (2006) 298-306.

V.V. Tyagi, S.C. Kaushik, S.K. Tyagi. Advancement in solar photovoltaic/thermal (PV/T) hybrid collector technology. Renewable and Sustainable Energy Reviews 16 (2012) 1383-1398.

W. Aziz, S.K. Chaturvedi, A. Kheireddine. Thermodynamic analysis of two-component, two-phase flow in solar collectors with application to a direct-expansion solar-assisted heat pump. Energy 24 (1999) 247-259.

Wei Pang, Qian Zhang, Yanan Cui, Linrui Zhang, Hongwen Yu, Xiaoyan Zhang, Yongzhe Zhang, Hui Yan. Numerical simulation and experimental validation of a photovoltaic/thermal system based on a roll-bond aluminum collector. Energy 187 (2019) 115990.

WORKING DOCUMENT Review of available information Accompanying the document Communication from the Commission to the European Parliament, the Council, the European Economic and Social Committee and the Committee of the Regions on an EU Strategy for Heating and Cooling {COM(2016) 51 final} https://ec.europa.eu/energy/sites/ener/files/documents/1_EN_autre_document_travail_service_part1_v6_0.pdf

Xiaolin Sun, Jingyi Wu, Yanjun Dai, Ruzhu Wang. Experimental study on roll-bond collector/evaporator with optimizedchannel used in direct expansion solar assisted heat pump water heating system. Applied Thermal Engineering 66 (2014) 571-579.

Yogi Goswami D. Principles of solar engineering. Third ed. CRC Press Tayolr &Francis Group; 2015.

Zahra Hajabdollahi, Hassan Hajabdollahi. Thermo-economic modeling and multi-objective optimization of solar water heater using flat plate collector. Solar Energy 155 (2017) 191-202.

Zheng Xinye, Ping Qin. 2014. “Characteristics of residential energy consumption in China: Findings from a household survey.” Energy Policy 75: 126-135.